Optics and Photonics Journal, 2015, 5, 326-333
Published Online November 2015 in SciRes. http://www.scirp.org/journal/opj
http://dx.doi.org/10.4236/opj.2015.511031

Large Redshifts in Emission and Excitation from Eu^{2+}-Activated Sr_2SiO_4 and Ba_2SiO_4 Phosphors Induced by Controlling Eu^{2+} Occupancy on the Basis on Crystal-Site Engineering

Yasushi Sato[1*], Hiroki Kuwahara[2], Hideki Kato[2], Makoto Kobayashi[2], Takaki Masaki[3], Masato Kakihana[2*]

[1]Department of Chemistry, Faculty of Science, Okayama University of Science, Okayama, Japan
[2]Institute of Multidisciplinary Research for Advanced Materials, Tohoku University, Sendai, Japan
[3]School of Advanced Materials Science and Engineering, Sungkyunkwan University, Suwon, Republic of Korea
Email: *satoy@chem.ous.ac.jp, *kakihana@tagen.tohoku.ac.jp

Received 17 October 2015; accepted 26 October 2015; published 25 November 2015

Abstract

The photoluminescence properties of Eu^{2+}-activated α'-Sr_2SiO_4 and α'-Ba_2SiO_4 with a high Eu^{2+} concentration were investigated. In the case of $Sr_{2-x}Eu_xSiO_4$, emission was shifted from 585 to 611 nm with increasing the total Eu^{2+} concentration (x) from 0.1 to 0.8. This trend was similar to that in $Ba_{2-x}Eu_xSiO_4$, where the emission was shifted from 513 to 545 nm. The large redshifts in both the excitation and emission spectra were discussed in terms of the Eu^{2+} occupancies on two kinds of M sites and their local structural changes (M: Sr and Ba).

Keywords

Photoluminescence, Red-Emitting Phosphors, Green-Emitting Phosphors, Orthosilicates, Crystal-Site Engineering

*Corresponding authors.

How to cite this paper: Sato, Y., Kuwahara, H., Kato, H., Kobayashi, M., Masaki, T. and Kakihana, M. (2015) Large Redshifts in Emission and Excitation from Eu^{2+}-Activated Sr_2SiO_4 and Ba_2SiO_4 Phosphors Induced by Controlling Eu^{2+} Occupancy on the Basis on Crystal-Site Engineering. *Optics and Photonics Journal*, **5**, 326-333. http://dx.doi.org/10.4236/opj.2015.511031

1. Introduction

Over the last decade, there have been many reports on the development of high-efficiency green- and red-emitting phosphors that respond to excitation by blue-LEDs as this is one of the greatest practical challenges associated with the realization of warm white-LED lamps [1]-[8]. Presently, silicon-based nitride and oxy-nitride phosphors, such as β-SiAlON:Eu^{2+}, $Ba_3Si_6O_{12}N_2$:Eu^{2+}, (Ca, Sr)$AlSiN_3$:Eu^{2+}, are the most suitable ones for white-LED applications [1] [3]-[5] because they possess excellent luminescent properties, low thermal quenching, and high chemical stability because of their high covalencies. However, they are usually prepared using refractory Si_3N_4 and unstable alkaline-earth nitrides as raw materials under high temperatures (>1500˚C) and high pressures (>0.1 MPa). Thus, their production efficiencies and costs are disadvantageous with regard to their commercial applications [9].

In contrast to nitride and oxy-nitride phosphors, the production of oxide phosphors is more convenient as it does not require refractory or unstable raw materials, and high temperatures and pressures. Therefore, silicon-based oxide phosphors that possess properties similar to those of nitride and oxy-nitride phosphors are promising alternatives as phosphors for next-generation white-LEDs.

Recently, several oxide phosphors with excellent luminescence properties have been reported [10]-[15]. Especially, the deep-red emitting Ca_2SiO_4:Eu^{2+} ($Ca_{1.2}Eu_{0.8}SiO_4$) [14] and the orange-red emitting $Sr_6Y_2Al_4O_{15}$:Ce^{3+} [15] has been prepared by the basis on crystal-site engineering [16]. In the case of $Ca_{1.2}Eu_{0.8}SiO_4$, this phosphor shows an emission peak at 653 nm under excitation at 450 nm [14]. The emission wavelength of $Ca_{1.2}Eu_{0.8}SiO_4$ is quite similar to those of typical red-emitting $CaAlSiN_3$:Eu^{2+} and $Sr_2Si_5N_8$:Eu^{2+} [4] [6]. $Ca_{1.2}Eu_{0.8}SiO_4$ has been identified as an α'_L-Ca_2SiO_4 structure (space group: $Pna2_1$, No. 33) with two types of calcium sites: viz. with coordination numbers of 10 [Ca(1*n*), *n* = 1 - 3] and 8 [Ca(2*n*), *n* = 1 - 3]. When a small amount of Eu^{2+} ions ($x < 0.20$) is added into $Ca_{2-x}Eu_xSiO_4$, most of the Eu^{2+} ions preferentially occupy the large Ca(1*n*) sites, showing green or green-yellow emission under UV light excitation [14]. However, upon adding a large amount of Eu^{2+} ions ($x > 0.20$) to the initial composition of $Ca_{2-x}Eu_xSiO_4$, Eu^{2+} substitution in the small Ca(2*n*) sites is promoted [14]. In the case of $Ca_{1.2}Eu_{0.8}SiO_4$, the Eu^{2+} occupancy in Ca(2*n*) sites was about 9% of the total concentration of Eu^{2+}. Thus, it is believed that a certain amount of Eu^{2+} substitution in the Ca(2*n*) sites led to the deep-red emission of $Ca_{1.2}Eu_{0.8}SiO_4$ at about 650 nm [14]. The crystal structure of $Ca_{2-x}Eu_xSiO_4$ is analogous to those of $Sr_{2-x}Eu_xSiO_4$ and $Ba_{2-x}Eu_xSiO_4$ [17]. Therefore, it is expected that the addition of large amounts of Eu^{2+} ions to $Sr_{2-x}Eu_xSiO_4$ and $Ba_{2-x}Eu_xSiO_4$ can lead to large redshift in their emission and excitation spectra. In this study, we prepared $Sr_{2-x}Eu_xSiO_4$ and $Ba_{2-x}Eu_xSiO_4$ with a high concentration of Eu^{2+} ions and characterized their structural and photoluminescence properties.

2. Experimental Detail

Polycrystalline $Sr_{1.2}Eu_{0.8}SiO_4$ and $Ba_{1.2}Eu_{0.8}SiO_4$ samples were synthesized by a conventional solid-state reaction method, using $SrCO_3$ or $BaCO_3$, Eu_2O_3 and SiO_2 powders as raw materials. These raw powders were mixed in stoichiometric proportions in ethanol by using an agate mortar. The resulting mixtures were calcined at 1000˚C in air for 12 h. Subsequently, the calcined powders were reground and mixed with a small amount of $BaCl_2$ as flux reagents. Finally, the powders were heat-treated in a tube furnace at 1200˚C for 4 h under a flow of an Ar (96%)-H_2 (4%) gas mixture with flow rate at 400 ml/min. In order to compare the Eu^{2+} occupancies and photoluminescence (PL) properties of $Sr_{1.2}Eu_{0.8}SiO_4$ and $Ba_{1.2}Eu_{0.8}SiO_4$, we also prepared $Sr_{1.9}Eu_{0.1}SiO_4$and $Ba_{1.2}Eu_{0.8}SiO_4$ samples with a low Eu^{2+} concentration by an amorphous metal complex (AMC) method using propylene glycol-modified silane [18]. This is because $Sr_{1.9}Eu_{0.1}SiO_4$ and $Ba_{1.2}Eu_{0.8}SiO_4$ samples prepared by a solid-state reaction method contained a large amount of impurities such as $SrCO_3$ or $BaCO_3$, compared with the samples prepared by the AMC method. These samples were then heat-treated by the same procedures as used for the $Sr_{1.2}Eu_{0.8}SiO_4$ and $Ba_{1.2}Eu_{0.8}SiO_4$ samples.

For single micrograins in $Sr_{1.2}Eu_{0.8}SiO_4$ and $Ba_{1.2}Eu_{0.8}SiO_4$ polycrystalline powders, quantitative analysis of metal elements such as Sr, Ba and Eu was firstly carried out by scanning electron microscopy (SEM, SU1510, Hitachi) together with energy-dispersive X-ray spectroscopy (EDS, X-act, Horiba). The applied voltage used for EDS analysis was 20 kV. Then, these final products were characterized by X-ray diffraction (XRD, D2 PHASER, *Bruker*AXS) using Cu-Kα radiation. XRD patterns were collected using the continuous scan mode with a step interval of 0.02˚. In the case of XRD measurements of samples containing higher concentrations of Eu, a significant increase in background signal was observed due to sample fluorescence. Therefore, XRD pat-

terns in these samples were measured with optimized discriminator settings to suppress the fluorescence effect [14]. PL spectra of $Sr_{1.2}Eu_{0.8}SiO_4$ and $Ba_{1.2}Eu_{0.8}SiO_4$ polycrystalline powders were analyzed using a fluorescence spectrometer (FP-8500, JASCO) equipped with an integrating sphere (ISF-513, JASCO).

3. Results and Discussion

Figure 1(a) and **Figure 1(b)** show the X-ray diffraction (XRD) patterns of $Sr_{2-x}Eu_xSiO_4$ and $Ba_{2-x}Eu_xSiO_4$ samples with total Eu^{2+} concentrations (x) of 0.1 and 0.8. Although trace amounts of $SrCO_3$ and $BaCO_3$ impurities were detected in the $Sr_{1.9}Eu_{0.1}SiO_4$ and $Ba_{1.9}Eu_{0.1}SiO_4$ samples, all samples were identified as orthorhombic α'-Sr_2SiO_4 structures with the *Pnma* (No. 62) space group [17] [19]. Subsequently, the XRD patterns were subjected to Rietveld refinement (RIETAN-FP program [20]) using the crystal structure of $Sr_{1.9}Ba_{0.1}SiO_4$ as a starting model structure [17]. Based on quantitative elemental analysis by energy-dispersive X-ray spectroscopy (EDS), the occupancies of Eu^{2+} in the M(1) and M(2) sites in $M_{2-x}Eu_xSiO_4$ (M: Sr and Ba) were also subjected to Rietveld refinement, as shown in **Table 1** and **Table 2**. Here, the total Eu^{2+} concentrations in both $Sr_{1.2}Eu_{0.8}SiO_4$ and $Ba_{1.2}Eu_{0.8}SiO_4$ after heat treatment with the $BaCl_2{\cdot}2H_2O$ flux were refined as 0.70, which was lower than that in the samples with initial compositions. This indicates that, during heat treatment, some amount of Eu^{2+} is exchanged by Ba^{2+} ions from $BaCl_2{\cdot}2H_2O$. Irrespective of the Eu^{2+} total concentration, the Sr(1) sites had higher Eu^{2+} occupancies than the Sr(2) sites. The percentage of the total Eu^{2+} occupancy in Sr(2) sites against Eu(1) sites increased significantly from 33% to 45% upon increasing the total Eu^{2+} concentration (x) from 0.1 to 0.8.

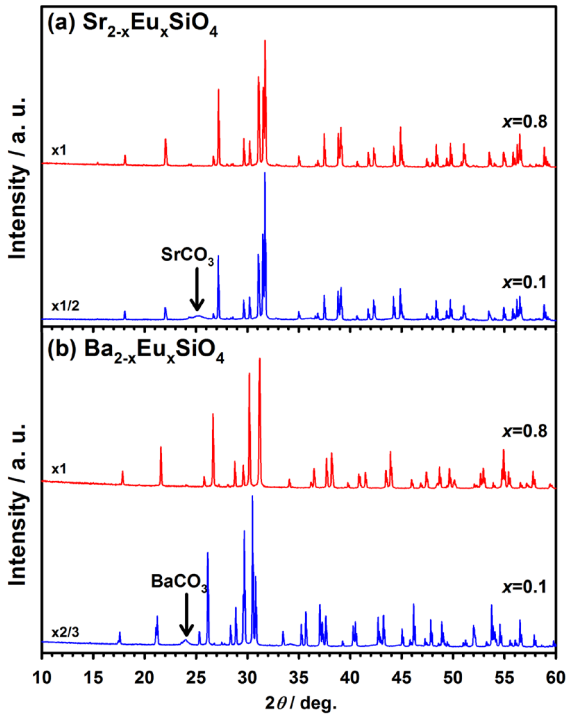

Figure 1. X-ray diffraction patterns of (a) $Sr_{2-x}Eu_xSiO_4$ (x = 0.1 and 0.8) and (b) $Ba_{2-x}Eu_xSiO_4$ (x = 0.1 and 0.8) polycrystalline samples.

Table 1. Lattice constants and Eu^{2+} occupancies at each Sr site of $Sr_{2-x}Eu_xSiO_4$ samples, estimated by Rietveld refinements of their X-ray diffraction patterns.

Total concentration of Eu^{2+} (x)	Lattice constants (Å)			Occupancy of Eu^{2+}		
	a	b	c	Total (Refinement)	Sr(1) site	Sr(2) site
0.10	7.1017	5.6724	9.7458	0.09	0.06	0.03
0.80	7.1090	5.6706	9.7502	0.70	0.38	0.32

Table 2. Lattice constants and Eu^{2+} occupancies at each Ba site of $Ba_{2-x}Eu_xSiO_4$ samples, estimated by Rietveld refinements of their X-ray diffraction patterns.

Total concentration of Eu^{2+} (x)	Lattice constants (Å)			Occupancy of Eu^{2+}		
	a	b	c	Total (Refinement)	Ba(1) site	Ba(2) site
0.10	7.4884	5.8014	10.1787	0.10	0.01	0.09
0.80	7.3691	5.7423	9.9205	0.70	0.15	0.55

Hence, the trend in $Sr_{2-x}Eu_xSiO_4$ is similar to that in $Ca_{2-x}Eu_xSiO_4$ [14]. On the other hand, the trend of variation in Eu^{2+} occupancies between the Ba(1) and Ba(2) sites in $Ba_{2-x}Eu_xSiO_4$ is opposite that in $Ca_{2-x}Eu_xSiO_4$ [14] and $Sr_{2-x}Eu_xSiO_4$, as shown in **Table 2**. Eu^{2+} ions predominantly occupy Ba(2) sites in $Ba_{1.9}Eu_{0.1}SiO_4$. However, as the total Eu^{2+} concentration is increased, Eu^{2+} ions occupy not only Ba(2) sites, but also Ba(1) sites.

Figure 2(a) and **Figure 2(b)** show the emission and excitation spectra of $Sr_{2-x}Eu_xSiO_4$ and $Ba_{2-x}Eu_xSiO_4$ samples with total Eu^{2+} concentrations (x) of 0.1 and 0.8. Broad emission peaks assigned to the $4f^65d^1 \rightarrow 4f^7$ transition of Eu^{2+} were observed for all the samples. As the total concentration of Eu^{2+} ions increased from 0.1 to 0.8, large emission redshifts were observed from 585 to 611 nm for $Sr_{2-x}Eu_xSiO_4$ and from 513 to 545 nm for $Ba_{2-x}Eu_xSiO_4$. On the other hand, the right-hand edges of the corresponding excitation spectra of both samples were shifted to longer wavelengths as the total Eu^{2+} concentration increased from 0.1 to 0.8. The increase in the widths of the right-hand edges in the excitation spectra were about 40 nm for $Ba_{2-x}Eu_xSiO_4$ and about 55 nm for $Sr_{2-x}Eu_xSiO_4$. The wavelength with the maximum excitation intensity was about 370 nm for both samples.

Figure 3(a) and **Figure 3(b)** show the emission and excitation spectra of $M_{1.2}Eu_{0.8}SiO_4$ samples (M: Ca, Sr, and Ba). Upon excitation at 450 nm, the emission peaks of $M_{1.2}Eu_{0.8}SiO_4$ were located at 653, 613, and 541 nm for Ca, Sr, and Ba, respectively. The wavelength with the maximum emission intensity was systematically shifted towards shorter wavelengths on moving towards alkaline earth elements with larger ionic radii (Ca → Sr → Ba) [21]. The intensities of $Sr_{1.2}Eu_{0.8}SiO_4$ and $Ba_{1.2}Eu_{0.8}SiO_4$ were approximately 1.6 times higher than that of $Ca_{1.2}Eu_{0.8}SiO_4$. The CIE chromaticity coordinates of the samples upon excitation at 450 are shown in **Figure 4**. The x (0.58) and y (0.42) coordinates of $Sr_{1.2}Eu_{0.8}SiO_4$ are comparable to that of red light. On the other hand, the x (0.39) and y (0.58) coordinates of $Ba_{1.2}Eu_{0.8}SiO_4$ are comparable to that of the green light region. The external and internal QE values for excitation at 450 nm were 46% and 58% for $Sr_{1.2}Eu_{0.8}SiO_4$ and 47% and 53% for $Ba_{1.2}Eu_{0.8}SiO_4$, respectively, which are similar to those for $Ca_{1.2}Eu_{0.8}SiO_4$ (external QE: 44% and internal QE: 50%) [14].

Finally, we discuss the origin of the large redshifts observed in the emission and excitation spectra of $Sr_{2-x}Eu_xSiO_4$ and $Ba_{2-x}Eu_xSiO_4$ on changing the total Eu^{2+} concentration (x) from 0.1 to 0.8 in terms of the occupancies of Eu^{2+} ions on the M(1) and M(2) sites and the local structural changes at both M sites (M: Sr and Ba). In the α'-Sr_2SiO_4 structure, the polyhedral volume of the M(1) sites is greater than that of the M(2) sites and the coordination numbers are 10 and 9, respectively [17] Based on the crystal parameters obtained from Rietveld refinement, the polyhedral volumes and distortion indices of the M(1) and M(2) sites in both samples were estimated by a VESTA program [22] using the methods suggested by Swanson and Peterson [23] and Baur [24]. The similar estimations for $Sr_xBa_{2-x}SiO_4$:Eu_{2+} (Eu^{2+} = 0.1) have been also reported by Denault *et al.* [25].

As is evident from **Table 3**, the polyhedra of the Sr(2) sites in $Sr_{2-x}Eu_xSiO_4$ were smaller and more distorted than those of the Sr(1) sites, regardless of Eu^{2+} concentration. If Eu^{2+} ions occupy the Sr(2) sites, the coordination environment of the Eu^{2+} ions can lead to strong crystal field splitting of the 5d orbitals of Eu^{2+} ions. Therefore, the red emission band (λ_{em} = 612 nm) observed in $Sr_{1.2}Eu_{0.8}SiO_4$ is mainly produced from the Eu^{2+} ions in Sr(2) sites, since a certain amount of Eu^{2+} ions is present in the Sr(2) sites. It is conceivable that the addition of a large amount of Eu^{2+} based on crystal-site engineering is mainly responsible for the large redshifts in the emission and excitation spectra of $Sr_{2-x}Eu_xSiO_4$. The relationship between PL properties and Eu^{2+} occupancy is quite similar to that in the case of $Ca_{2-x}Eu_xSiO_4$ [14]. In contrast, the yellow emission band (λ_{em} = 585 nm) observed in $Sr_{1.9}Eu_{0.1}SiO_4$ was composed of at least two emission peaks: one originating from the Sr(1) sites and the other from the Sr(2) sites. It is plausible that the main contribution to the yellow emission band was from emissions originating from the Sr(1) sites, since most of the Eu^{2+} ions occupied Sr(1) sites in $Sr_{1.9}Eu_{0.1}SiO_4$, as shown in **Table 1**.

The polyhedral volumes and distortion indices of $Ba_{2-x}Eu_xSiO_4$ samples with total Eu^{2+} concentrations (x) of 0.1 and 0.8 are listed in **Table 4**. The polyhedral volume of the Ba(2) sites in $Ba_{1.2}Eu_{0.8}SiO_4$ is smaller than that

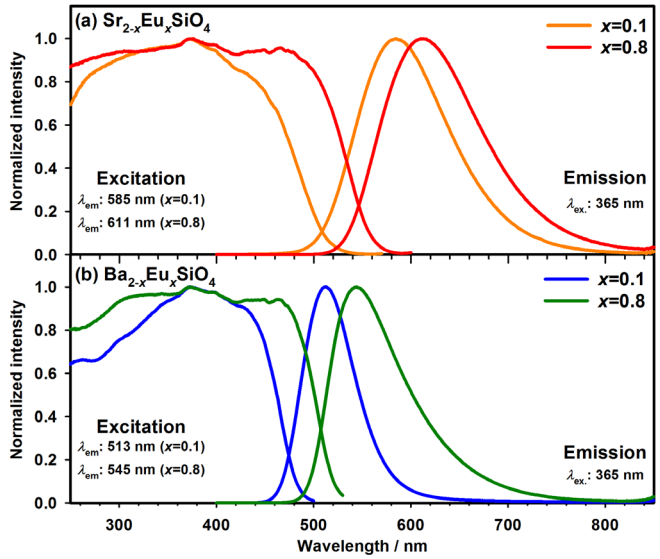

Figure 2. Emission (λ_{ex} = 365 nm) and excitation spectra of (a) $Sr_{2-x}Eu_xSiO_4$ and (b) $Ba_{2-x}Eu_xSiO_4$ with total Eu^{2+} concentrations (x) of 0.1 and 0.8. The intensities of the emission and excitation spectra were normalized according to the maximum intensity of the spectra.

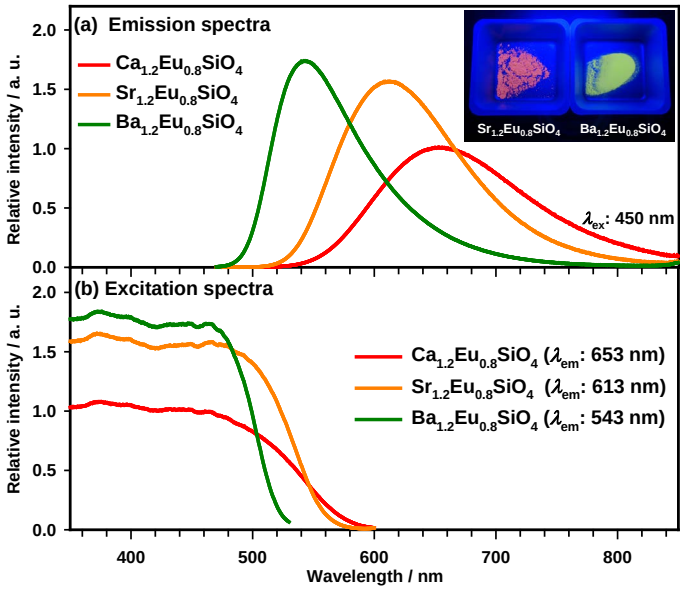

Figure 3. (a) Emission (λ_{ex} = 450 nm) and (b) excitation spectra of $Sr_{1.2}Eu_{0.8}SiO_4$ and $Ba_{1.2}Eu_{0.8}SiO_4$. For comparison, the emission and corresponding excitation spectra of $Ca_{1.2}Eu_{0.8}SiO_4$ are also shown in both the figures. The photographs of $Sr_{1.2}Eu_{0.8}SiO_4$ and $Ba_{1.2}Eu_{0.8}SiO_4$ phosphors upon blue-light excitation with blue LED are inserted in **Figure 3(a)**.

Table 3. Polyhedral volumes and distortion indices of the Sr(1) and Sr(2) sites in $Sr_{2-x}Eu_xSiO_4$ samples (total Eu^{2+} concentration (x) equal to 0.1 and 0.8).

Total concentration of Eu^{2+} (x)	Polyhedral volume (Å^3)		Distortion index	
	Sr(1) site	Sr(2) site	Sr(1) site	Sr(2) site
0.10	46.903	37.267	0.0388	0.0652
0.80	47.710	36.538	0.0425	0.0687

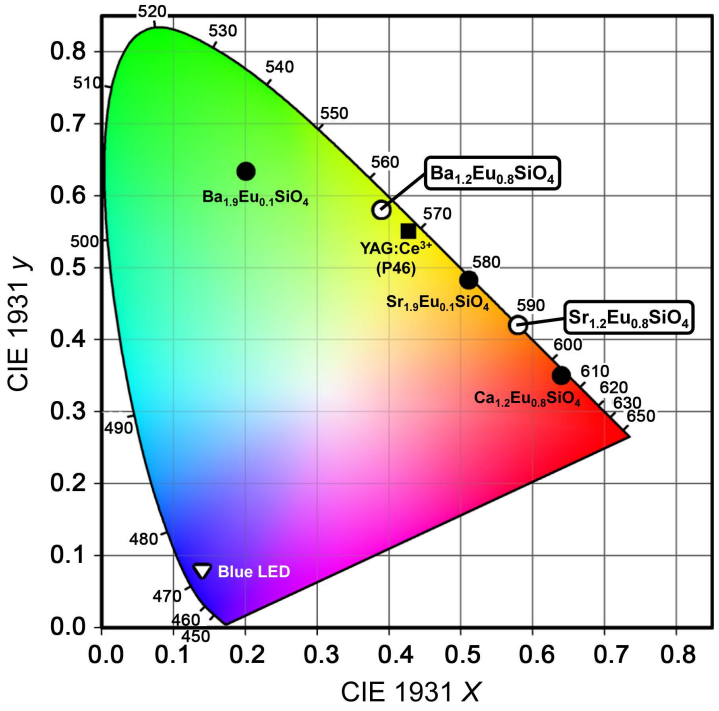

Figure 4. The CIE chromaticity coordinates of $Sr_{1.2}Eu_{0.8}SiO_4$ and $Ba_{1.2}Eu_{0.8}SiO_4$ phosphors (open circles). The coordinates of three other orthosilicate phosphors ($Ca_{1.2}Eu_{0.8}SiO_4$, $Sr_{1.9}Eu_{0.1}SiO_4$ and $Ba_{1.9}Eu_{0.1}SiO_4$: solid circles), commercial YAG:Ce^{3+} (P46) phosphors (solid square), and blue LEDs (open triangle) are also shown in this figure.

Table 4. Polyhedral volumes and distortion indices of the Ba(1) and Ba(2) sites in $Ba_{2-x}Eu_xSiO_4$ samples (total Eu^{2+} concentration (x) equal to 0.1 and 0.8).

Total concentration of Eu^{2+} (x)	Polyhedral volume (Å^3)		Distortion index	
	Ba(1) site	Ba(2) site	Ba(1) site	Ba(2) site
0.10	53.244	43.064	0.0437	0.0475
0.80	51.431	39.356	0.0418	0.0584

in $Ba_{1.9}Eu_{0.1}SiO_4$. In addition, the distortion index of the Ba(2) sites in $Ba_{1.2}Eu_{0.8}SiO_4$ is larger than that in $Ba_{1.9}Eu_{0.1}SiO_4$, while the distortion index of the Ba(1) sites in $Ba_{1.2}Eu_{0.8}SiO_4$ and $Ba_{1.9}Eu_{0.1}SiO_4$ is almost the same. Therefore, the large redshifts in both the excitation and emission spectra of $Ba_{2-x}Eu_xSiO_4$ could be attributed to the decrease in polyhedral volume and the increase in distortion of the Ba(2) site. This trend for $Ba_{2-x}Eu_xSiO_4$ matches with that for intermediate compositions of the solid-solution $Ba_{2-x}Sr_xSiO_4$:Eu^{2+} [25].

4. Conclusion

We observed large redshifts in both the emission and excitation spectra of $M_{2-x}Eu_xSiO_4$ (M: Sr and Ba) at high concentration of Eu^{2+} ions. In the case of $Sr_{2-x}Eu_xSiO_4$, the emission peak was shifted from 585 nm for $Sr_{1.9}Eu_{0.1}SiO_4$ to 611 nm for $Sr_{1.2}Eu_{0.8}SiO_4$. On the other hand, in the case of $Ba_{2-x}Eu_xSiO_4$, the emission peak was shifted from 513 nm for $Ba_{1.9}Eu_{0.1}SiO_4$ to 545 nm for $Ba_{1.2}Eu_{0.8}SiO_4$. The right-hand edges of the excitation spectra for both the samples were significantly shifted by 40 - 55 nm to longer wavelengths, allowing for excitation by blue light. The induction of large redshifts in the emission and excitation spectra of both samples could be attributed to the occupancy of Eu^{2+} ions in the polyhedra of Sr(2) or Ba(2) sites, which is smaller and more distorted than the Sr(1) or Ba(1) sites. These results indicate that $Sr_{1.2}Eu_{0.8}SiO_4$ and $Ba_{1.2}Eu_{0.8}SiO_4$ are suitable as red- and green-emitting phosphors for next-generation white-LED applications.

Acknowledgements

This work was partially supported by a Grant-in-Aid for Scientific Research (No. 22107002) on Innovative Areas of "Fusion Materials: Creative Development of Materials and Exploration of Their Function through Molecular Control" from the Ministry of Education, Culture, Sports, Science and Technology, Japan (MEXT). This work was also partially supported by the Cooperative Research Program of the "Network Joint Research Center for Materials and Devices".

References

[1] Hirosaki, N., Xie, R.-J., Kimoto, K., Sekiguchi, T., Yamamoto, Y., Suehiro, T. and Mitomo, M. (2005) Characterization and Properties of Green-Emitting β-SiAlON:Eu^{2+} Powder Phosphors for White Light-Emitting Diodes. *Applied Physical Letters*, **86**, Article ID: 211905.

[2] Shimomura, Y., Honma, T., Shigeiwa, M., Akai, T., Okamoto, K. and Kijima, N. (2007) Photoluminescence and Crystal Structure of Green-Emitting $Ca_3Sc_2Si_3O_{12}$:Ce^{3+} Phosphor for White Light Emitting Diodes. *Journal of the Electrochemical Society*, **154**, J35-J38. http://dx.doi.org/10.1149/1.2388856

[3] Yun, B.-G., Horikawa, T., Hanzawa, H. and Machida, K. (2010) Preparation and Luminescence Properties of Single-Phase $BaSi_2O_2N_2$:Eu^{2+}, a Bluish-Green Phosphor for White Light-Emitting Diodes. *Journal of the Electrochemical Society*, **157**, J364-J370. http://dx.doi.org/10.1149/1.3479763

[4] Uheda, K., Hirosaki, N., Yamamoto, Y., Naito, A., Nakajima, T. and Yamamoto, H. (2006) Luminescence Properties of a Red Phosphor, $CaAlSiN_3$:Eu^{2+}, for White Light-Emitting Diodes. *Electrochemical and Solid-State Letters*, **9**, H22-H25. http://dx.doi.org/10.1149/1.2173192

[5] Watanabe, H., Yamane, H. and Kijima, N. (2008) Crystal Structure and Luminescence of $Sr_{0.99}Eu_{0.01}AlSiN_3$. *Journal of Solid State Chemistry*, **181**, 1848-1852. http://dx.doi.org/10.1016/j.jssc.2008.04.017

[6] Xie, R.J., Hirosaki, N., Suehiro, T., Xu, F.F. and Mitomo, M. (2006) A Simple, Efficient Synthetic Route to $Sr_2Si_5N_8$:Eu^{2+}-Based Red Phosphors for White Light-Emitting Diodes. *Chemistry of Materials*, **18**, 5578-5583. http://dx.doi.org/10.1021/cm061010n

[7] Park, W.B., Singh, S.P., Yoon, C. and Sohn, K.-S. (2012) Eu^{2+} Luminescence from 5 Different Crystallographic Sites in a Novel Red Phosphor, $Ca_{15}Si_{20}O_{10}N_{30}$:$Eu^{2+}$. *Journal of Materials Chemistry*, **22**, 14068-14075. http://dx.doi.org/10.1039/c2jm32032k

[8] Pust, P., Weiler, V., Hecht, C., Tücks, A., Wochnik, A.S., Henß, A., Wiechert, D., Scheu, C., Schmidt, P.J. and Schnick, W. (2014) Narrow-Band Red-Emitting $Sr[LiAl_3N_4]$:Eu^{2+} as a Next-Generation LED-Phosphor Material. *Nature Materials*, **13**, 891-896. http://dx.doi.org/10.1038/nmat4012

[9] Setlur, A.A. (2009) Phosphors for LED-Based Solid-State Lighting. *The Electrochemical Society Interface*, **18**, 32-36. http://test.electrochem.org/dl/interface/wtr/wtr09/wtr09_p032-036.pdf

[10] Daicho, H., Iwasaki, T., Enomoto, K., Sasaki, Y., Maeno, Y., Shinomiya, Y., Aoyagi, S., Nishibori, E., Sakata, M., Sawa, H., Matsuishi, S. and Hosono, H. (2012) A Novel Phosphor for Glareless White Light-Emitting Diodes. *Nature Communications*, **3**, Article ID: 1132.

[11] Tezuka, S., Sato, Y., Komukai, T., Takatsuka, Y., Kato, H. and Kakihana, M. (2013) Eu^{2+}-Activated $CaSrSiO_4$: A New Red-Emitting Oxide Phosphor for White-Light-Emitting Diodes. *Applied Physics Express*, **6**, Article ID: 072101.

[12] Kim, S.W., Hasegawa, T., Ishigaki, T., Uematsu, K., Toda, K. and Sato, M. (2013) Efficient Red Emission of Blue-Light Excitable New Structure Type $NaMgPO_4$:Eu^{2+} Phosphor. *ECS Solid State Letters*, **2**, R49-R51. http://dx.doi.org/10.1149/2.004312ssl

[13] Huang, C.-H., Liu, W.-R., Chan, T.-S. and Lai, Y.-T. (2014) Orangish-Yellow-Emitting $Ca_3Si_2O_7$:Eu^{2+} Phosphor for Application in Blue-Light Based Warm-White LEDs. *Dalton Transactions*, **43**, 7917-7923. http://dx.doi.org/10.1039/c4dt00076e

[14] Sato, Y., Kato, H., Kobayashi, M., Masaki, T., Yoon, D.-H. and Kakihana, M. (2014) Tailoring of Deep-Red Luminescence in Ca_2SiO_4:Eu^{2+}. *Angewandte Chemie International Edition*, **53**, 7756-7759. http://dx.doi.org/10.1002/anie.201402520

[15] Kawano, Y., Kim, S.W., Ishigaki, T., Uematsu, K., Toda, K., Takaba, H. and Sato, M. (2014) Site Engineering Concept of Ce^{3+}-Activated Novel Orange-Red Emission Oxide Phosphors. *Optical Materials Express*, **4**, 1770-1774. http://dx.doi.org/10.1364/OME.4.001770

[16] Funakubo, H., Watanabe, T., Kojima, T., Sakai, T., Noguchi, Y., Miyayama, M., Osada, M., Kakihana, M. and Saito, K. (2003) Property Design of $Bi_4Ti_3O_{12}$-based Thin Films using a Site-engineered Concept. *Journal of Crystal Growth*, **248**, 180-185. http://dx.doi.org/10.1016/s0022-0248(02)02047-x

[17] Catti, M., Gazzoni, G. and Ivaldi, G. (1983) Structures of Twinned β-Sr_2SiO_4 and of α'-$Sr_{1.9}Ba_{0.1}SiO_4$. *Acta Crystallographica Section C*: *Structural Chemistry*, **39**, 29-34. http://dx.doi.org/10.1107/S0108270183003492

[18] Kakihana, M., Kim, J., Komukai, T., Kato, H., Sato, Y., Kobayashi, M. and Takatsuka, Y. (2013) Exploration of New Phosphors Using a Mineral-Inspired Approach in Combination with Solution Parallel Synthesis. *Optics and Photonics Journal*, **3**, 5-12. http://dx.doi.org/10.4236/opj.2013.36A002

[19] Poort, S.H.M., Janssen, W. and Blasse, G. (1997) Optical Properties of Eu^{2+}-Activated Orthosilicates and Orthophosphates. *Journal of Alloys and Compounds*, **260**, 93-97.

[20] Izumi, F. and Momma, K. (2007) Three-Dimensional Visualization in Powder Diffraction. *Solid State Phenomena*, **130**, 15-20. http://dx.doi.org/10.4028/www.scientific.net/SSP.130.15

[21] Shannon, R.D. (1976) Revised Effective Ionic Radii and Systematic Studies of Interatomic Distances in Halides and Chalcogenides. *ActaCrystallographica Section A*: *Foundations and Advances*, **32**, 751-767. http://dx.doi.org/10.1107/S0567739476001551

[22] Momma, K. and Izumi, F. (2011) VESTA 3 for Three-Dimensional Visualization of Crystal, Volumetric and Morphology Data. *Journal of Applied Crystallography*, **44**, 1272-1276. http://dx.doi.org/10.1107/S0021889811038970

[23] Swanson, D. and Peterson, R. (1980) Polyhedral Volume Calculations. *Canadian Mineralogist*, **18**, 153-156. http://www.canmin.org/content/18/2/153.full.pdf+html

[24] Baur, W.H. (1974) The Geometry of Polyhedral Distortions. Predictive Relationships for the Phosphate Group. *Acta Crystallographica Section B*: *Structural Crystallography and Crystal Engineering and Materials*, **30**, 1195-1215. http://dx.doi.org/10.1107/S0567740874004560

[25] Denault, K.A., Brgoch, J., Gaultois, M.W., Mikhailovsky, A., Petry, R., Winkler, H., Denbaars, S.P. and Seshadri, R. (2014) Consequences of Optimal Bond Valence on Structural Rigidity and Improved Luminescence Properties in $Sr_xBa_{2-x}SiO_4$:Eu^{2+} Orthosilicate Phosphors. *Chemistry of Materials*, **26**, 2275-2282. http://dx.doi.org/10.1021/cm500116u